Blending Through-Space and Through-Bond $\pi-\pi$-Coupling in [2,2']-Paracyclophane-oligophenylenevinylene Molecular Wires

Mateusz Wielopolski,[†,⊥] Agustín Molina-Ontoria,[‡,⊥] Christina Schubert,[†,⊥] Johannes T. Margraf,[†] Evangelos Krokos,[†] Johannes Kirschner,[†] Andreas Gouloumis,[‡] Timothy Clark,[§] Dirk M. Guldi,*[,†] and Nazario Martín*[,‡,∥]

[†]Department of Chemistry and Pharmacy & Interdisciplinary Center for Molecular Materials (ICMM), Friedrich-Alexander-Universität Erlangen-Nürnberg, Egerlandstrasse 3, 91058 Erlangen, Germany

[‡]Departamento de Química Orgánica, Facultad de Química, Universidad Complutense, E-28040 Madrid, Spain

[§]Computer-Chemie-Centrum, Department of Chemistry and Pharmacy & Interdisciplinary Center for Molecular Materials (ICMM), Friedrich-Alexander-Universität Erlangen-Nürnberg, Nägelsbachstr. 25, 91052 Erlangen, Germany

[∥]IMDEA-Nanociencia, Campus de Cantoblanco, E-28049 Madrid, Spain

Ⓢ *Supporting Information*

ABSTRACT: A series of ZnP-pCp-oPPV-C_{60} conjugates covalently connected through [2,2']-paracyclophane-oligophenylenevinylene (pCp-oPPV) bridges containing one, two, and three [2,2']-paracyclophanes (pCps) has been prepared in multistep synthetic procedures involving Horner−Wadsworth−Emmons olefination reactions and/or Heck type Pd-catalyzed reactions. Molecular modeling suggests that charge transfer is effectively mediated by the pCp-oPPVs through a predominant hole-transfer mechanism. Photophysical investigation supports molecular modeling and reveals two major trends. On one hand, C_{60} excitation of **1**, **2**, and **3** leads exclusively to charge transfer between pCp and C_{60} to afford a ZnP-(pCp-oPPV)$^{•+}$-$C_{60}$$^{•−}$ radical ion pair state without giving rise to a subsequent charge shift to yield the ZnP$^{•+}$-pCp-oPPV-$C_{60}$$^{•−}$ radical ion pair state. On the other hand, ZnP excitation of **1**, **2**, and **3** results in a rather slow charge transfer between ZnP and C_{60}, after which the ZnP$^{•+}$-pCp-oPPV-$C_{60}$$^{•−}$ radical ion pair state evolves. In temperature-dependent ZnP fluorescence experiments, which were performed in the temperature range from 273 to 338 K, two domains are discernible: low and high temperature behaviors. In the low temperature range (i.e., below 30 °C) the rate constants do not change, suggesting that a superexchange mechanism is the modus operandi. In the high temperature range (i.e., >30 °C) the rate constants increase. Moreover, we find rather strong distance dependence for **1** and **2** and weak distance dependence for **2** and **3**. A damping factor of 0.145 Å$^{−1}$ is derived for the former pair and 0.012 Å$^{−1}$ for the latter.
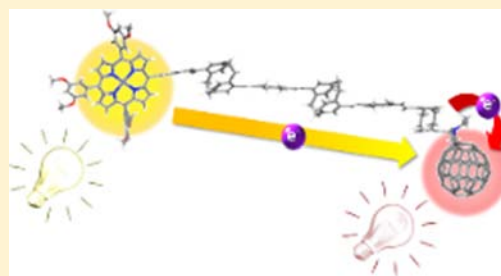
INTRODUCTION

Natural photosynthetic processes exhibit state-of-the-art efficiencies in terms of charge transfer to create electrochemical potentials and utilization thereof to drive chemical reactions.[1,2] Organic photovoltaic applications require precise control over charge-transfer rates to achieve maximum quantum yields. Hence, the natural photosynthetic system serves as a unique model for artificial solar energy conversion systems and for probing charge-transfer processes on the molecular scale. In this regard, a plethora of artificial photosynthetic mimics have been developed, in which the rates of light-induced charge transfer, that is, charge separation (k_{CS}) and charge recombination (k_{CR}), have been fine-tuned.[3−6] For long-lived charge separation to occur, the subtle interplay between different parameters is the key challenge, especially with increasing complexity of the molecular electron donor−acceptor conjugate/hybrid. The case of interfacing electron donors and electron acceptors with molecular wires creates a unique class of photosynthetic model systems for which

different synthetic methodologies provide a structural tool for fine-tuning the charge-transfer rates and to study the photoinduced charge transfer on a rather simplified level.

Porphyrins, on one hand, often constitute the electron donors in these electron donor−acceptor conjugates/hybrids due to the relative ease of synthesis, chemical stability, and excellent light absorption properties.[7] The electron acceptor, on the other hand, is in many photosynthetic model systems C_{60}, which has been shown to feature ideal electron acceptor properties.[8] Finally, the molecular wire is meant to ensure the electronic coupling between the electroactive termini, namely donors and acceptors.[9] It has been shown that by varying the chemical structure of the molecular wire that links donor and acceptor it is possible to gain control over charge transfer rates and the charge transfer mechanism, that is, superexchange versus hopping.[10,11] A key factor is hereby the π-conjugation,

not only within the molecular wire itself but also between the molecular wire and the electroactive termini. Notably, the ultimate goal in all of these electron donor−acceptor systems is to transfer electrons from the donors to the acceptors at a maximum rate, while slowing down the charge recombination as much as possible—$k_{CS} \gg k_{CR}$.[12]

Recently, we have documented that inserting single [2,2′]-paracyclophanes (pCp) with distinct through-space π–π-interactions into highly conjugated oligo-*p*-phenylenevinylenes (oPPV) affects the electron-mediating properties of oPPVs.[13] In pCp, the close proximity between the arenes results in strong electronic and structural interactions. As a matter of fact, styryl-[2,2′]-paracyclophanes exhibit highly conductive behavior and efficient through-space π–π coupling.[14] In pCp-oPPV conjugates, the pCps impose a molecular junction behavior, which accelerates k_{CS} and slows down k_{CR}.[13]

On the basis of our earlier work, which describes the charge transport in ZnP-C_{60} electron donor−acceptor conjugates bridged by [2,2]-paracyclophane-oligophenylenevinylene (pCp-oPPV) of different oPPV lengths, we present here the charge transport properties through pCp-oPPV wires comprising multiple pCps, that is, one, two, and three (Chart 1). By

Chart 1. ZnP-pCp-oPPV-C_{60} 1−3
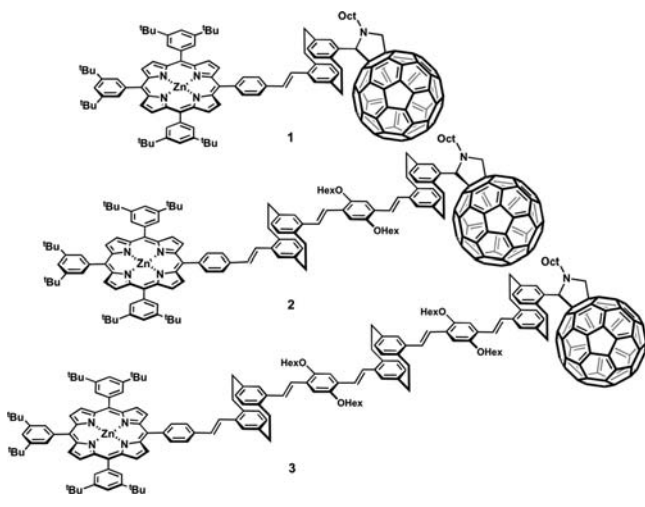
implementing a second and a third pCp we expected to introduce additional junctions into the oPPVs and favor a charge hopping mechanism over a superexchange mechanism. Importantly, such a change in mechanism is thought to impact the charge transfer rates, especially the charge recombination, and, in turn, to increase the charge separated state lifetimes. Apart from investigations by means of time-resolved spectroscopies on the femto- and nanosecond time scales, temperature-dependent steady-state experimental techniques were employed to survey the rate constants for intramolecular charge transfer occurring after photoexcitation. The latter are keys in distinguishing between superexchange and hopping charge transfer mechanisms. As a complement to the experimental approach, molecular modeling calculations were carried out to assess the electronic perturbations imposed on the oPPV electronic structure upon insertion of one, two, and three pCps.

■ RESULTS AND DISCUSSION

Synthesis. **2** and **3** were prepared in multistep synthetic procedures following a well-established procedure involving

[2,2′]-paracyclophane (pCp), zinc porphyrin (ZnP), and fullerene (C_{60})—see Supporting Information for details. The precursor dialdehydes **12** and **19** bearing two and three pCp units, respectively, were prepared in turn by using Horner−Wadsworth−Emmons olefination reactions and/or Heck type Pd-catalyzed reactions. In a subsequent synthetic step, ZnPs were covalently connected to the dialdehydes (**12**, **19**) by applying similar synthetic methodologies affording **13** and **20**, respectively. Finally, **2** and **3** were obtained by 1,3-dipolar cycloaddition reactions from the corresponding azomethine ylides, which were generated in situ from *N*-octylglycine and aldehydes **13** and **20**, respectively, to C_{60}, following Prato's protocol.[15] **1** was prepared by following the method previously reported by our group—Scheme 1.[16]

Electrochemistry. The electrochemical properties of **1**, **2**, and **3** and the references ZnP and pCp-C_{60} have been investigated by cyclic voltammetry (CV) at room temperature in THF and in *ortho*-dichlorobenzene, as shown in Figure S1 and Tables S1 and S2 (Supporting Information). In the cathodic scan sweep, **1**, **2**, and **3** exhibit four reduction waves at −0.84, −1.41, −1.73, and −2.03 V. The first, second, and fourth reversible one-electron reductions agree with the C_{60} reduction in the C_{60}-pCp reference. The third quasi-reversible one electron reduction wave corresponds to the ZnP reduction, which is in excellent agreement with the reference ZnP. In the anodic scan, **1**, **2**, and **3** show the quasi-reversible one-electron oxidation wave of ZnP (0.54 V). Additional experiments were performed in *ortho*-dichlorobenzene to determine the second ZnP-based oxidation potential and oxidations derived from the molecular wire (Table S1, Supporting Information). Upon careful examination of all of the redox data we conclude that no significant electronic interactions exist between the different redox- and photoactive constituents in **1**, **2**, and **3** in the ground state.

Molecular Modeling. Density functional theory (DFT) and semiempirical molecular orbital (MO) theory were used to characterize the geometrical and electronic properties of **1**, **2**, and **3** and their impact on their charge-transfer behavior. All geometry optimizations were performed using the hybrid B3LYP[17] exchange-correlation functional with the 6-31G(d)[18] basis set as implemented in the Gaussian09[19] program package. In order to complete the study, references **12**, **15**, **18**, **19**, **19**-C_{60},[20] **20**, and a pCp-C_{60} analogue were also investigated at the same level of theory.

The resulting molecular geometries of **1**, **2**, and **3** revealed dihedral angles between the pCps and the phenylenevinylene (oPPV) phenyl rings in the bridge moieties of 31−45°—Figure S2 (Supporting Information). The ZnP donors are nearly perpendicular (∼70°) to the plane of the π-spacers, which implies only 34% of the effective planar overlap. Therefore, the ZnPs are essentially electronically decoupled. The dihedral angles between the pCps and the oPPVs decrease with increasing bridge length from **1** to **3**, because the length of the π-conjugated system increases and the gain in enthalpy due to the planarization is greater than the steric hindrance.

The absence of total planarity between the pCps and oPPVs and ZnP and the bridge structure strongly impacts the electronic properties and the communication between the ZnP electron donor and the C_{60} electron acceptor, which varies with the length of the π-conjugated spacer. The frontier orbitals shown in Figure 1 illustrate the impact of structure on the electronic features of the systems.

Scheme 1. Synthesis of 1−3[a]
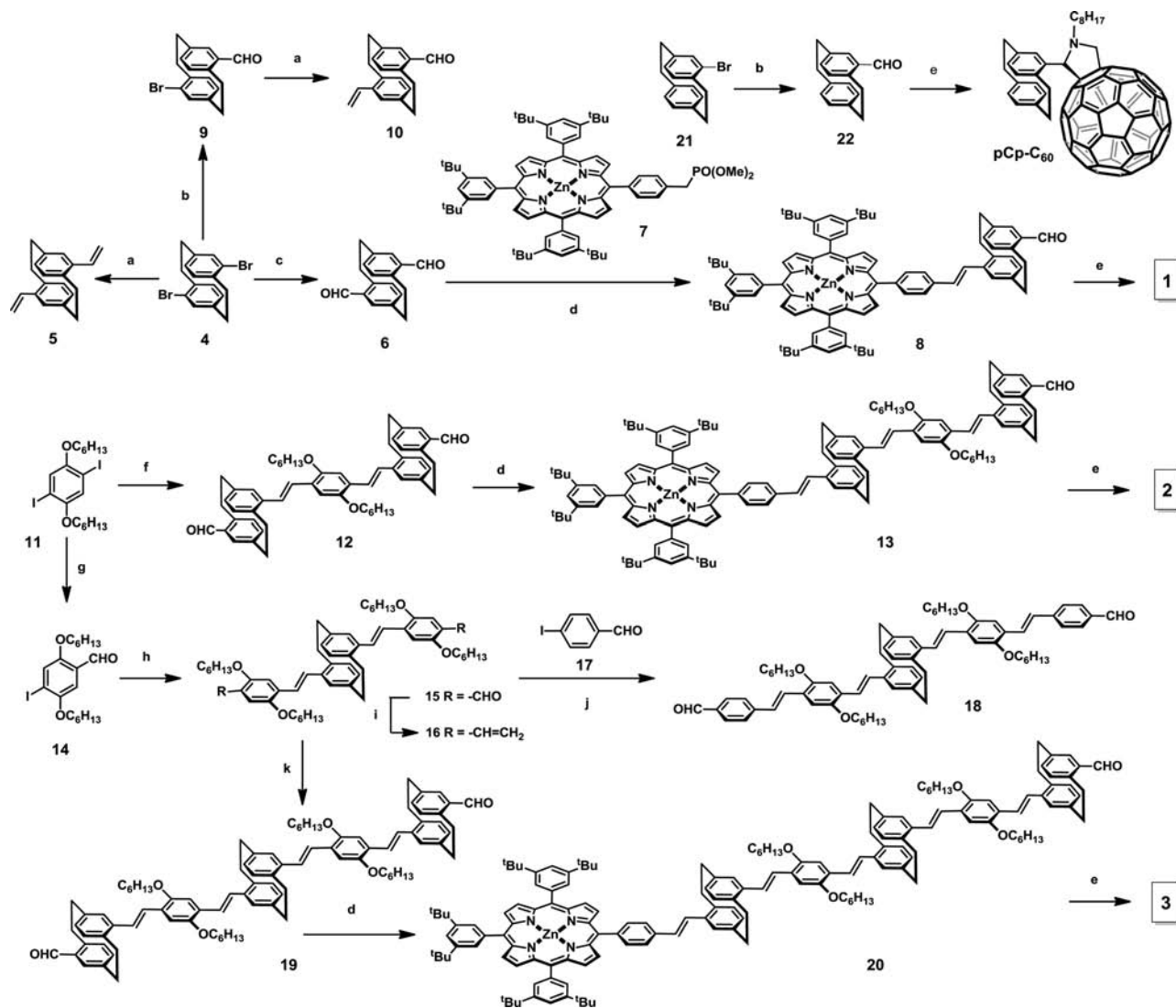
[a]Reagents and conditions: (a) Pd(PPh₃)₄, tributylvinyltin, toluene, 100 °C, 12 h, y = 89−92%; (b) n-BuLi (1.5 equiv), DMF (1.5 equiv) THF, −78 °C, to RT, 3 h, y = 75%; (c) sec-BuLi (2.2 equiv), ether/THF, −78 °C, DMF (2.2 equiv) to RT, 16 h, y = 55%; (d) 7 (0.5 equiv), tBuOK, dry THF, reflux, 2 h, y = 41−49%; (e) C₆₀, N-octylglycine, ClPh, reflux, 7 h, y = 39−40%; (f) 10 (2 equiv), Pd(OAc)₂, Bu₄NBr, K₂CO₃, DMF, 100 °C, 4h, y = 79%; g) n-BuLi (1.1 equiv), DMF (1.1 equiv) THF, 0 °C, 2 h, y = 75%; (h) 5 (0.5 equiv), Pd(OAc)₂, Bu₄NBr, K₂CO₃, DMF, 100 °C, 6 h, y = 81%; (i) Tebbe reagent (2.2 equiv), pyridine (cat.), THF, 0 °C, 2 h, y = 90%; (j) 17 (2 equiv), Pd(OAc)₂, Bu₄NBr, K₂CO₃, DMF, 100 °C, 8 h, y = 75%; (k) 9 (2.2 equiv), Pd(OAc)₂, Bu₄NBr, K₂CO₃, DMF, 100 °C, 4 h, y = 63%.

Hence, the highest occupied molecular orbital (HOMO) in **1** is quite localized on the ZnP donor due to the dihedral angle of nearly 70°. However, the HOMO orbital coefficients extend into the π-spacer, suggesting significant interactions with the bridge orbitals. As the length of the spacer increases, the coupling of the HOMO into the bridge is enhanced due to a lowering of the energies of the bridge orbitals upon increasing π-interactions. As a consequence, the HOMO in **2** is delocalized throughout the entire bridge. In **3**, on the other hand, the large distance between ZnP and C₆₀ localizes the HOMO on the bridge with some small coefficients on ZnP, whereas in **1** and **2** the main contribution to the HOMO and lower orbitals (HOMO-1 to HOMO-3) still resides on the ZnP donor. Consequently, localization of the bridge states is most pronounced in **3**. The lowest unoccupied molecular orbitals (LUMO) are localized on C₆₀. Interestingly, strong through-space π-interactions in the pCps allow π-conjugation to

continue through the Cp system. This was further corroborated by analyzing the HOMO and LUMO of **18**—Figure 2—where a complete conjugation throughout the entire structure is observed.

The effect of increasing π-conjugation upon increasing length of the spacer is clearly visible in the energies of the frontier orbitals—Table S3 (Supporting Information). Whereas in **1** the HOMO to HOMO-2 orbitals are separated by gaps of 0.14−0.43 eV, respectively, these values decrease for **2** and **3** to the range of 0.03−0.09 eV, indicating strong π-interactions.

Reference compounds pCp-C₆₀, **18**, **19**-C₆₀, and **20** were used to analyze the electron donating and accepting features of the different building blocks ZnP, C₆₀, oPPV, and pCp. As mentioned above, when neither ZnP nor C₆₀ is present (**18**), the electron density is evenly distributed throughout the entire molecule, and the through-space conjugation across the pCps allows sufficient electronic communication to guarantee π-
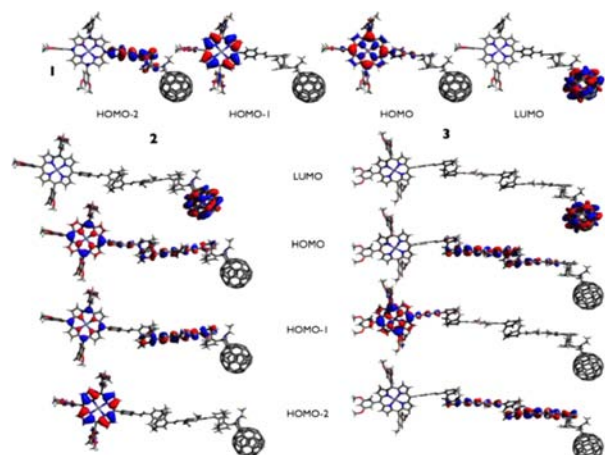
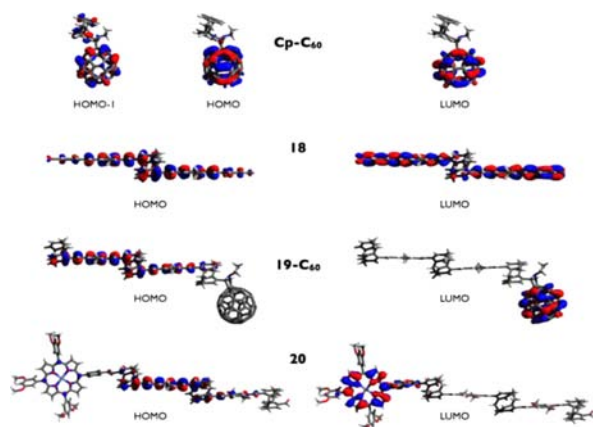**Figure 1.** Representative frontier orbitals of ZnP-oPPV-pCp-C$_{60}$ **1**, **2**, and **3** (B3LYP/6-31G(d)).

Figure 2. Representative frontier orbitals of pCp-C$_{60}$, **18**, **19**-C$_{60}$, and **20** (B3LYP/6-31G(d)).

overlap throughout the whole molecular structure. pCp-C$_{60}$, **19**-C$_{60}$, and **20** allow the electron donating and electron accepting features of the building blocks to be evaluated. As seen in Figure 2, the LUMOs of both pCp-C$_{60}$ and **19**-C$_{60}$ are localized on C$_{60}$, consistent with its electron accepting features. A comparison of the HOMOs between pCp-C$_{60}$ and **19**-C$_{60}$ shows that elongating the bridge increases the spatial separation of the HOMO and LUMO. In pCp-C$_{60}$, the HOMO-1 exhibits electron density contributions on the Cp, but significant electronic coupling to C$_{60}$ remains because of the short distance between C$_{60}$ and Cp. The HOMO in **19**-C$_{60}$, on the other hand, is entirely decoupled from the LUMOs, indicating that a long bridge moiety can act as a more efficient electron donor than a single Cp unit. Indeed, the evidently smaller HOMO to LUMO energy gap of 1.72 eV in **19**-C$_{60}$ may render an intramolecular electron transfer from the bridge to C$_{60}$ easier than in pCp-C$_{60}$ with its energy gap of 2.63 eV. The electron-donating properties of the Cp-oPPVs are further corroborated by considering the HOMOs and LUMOs of **20**, where the ZnP takes the role of the electron acceptor, with the HOMO remaining localized on the bridge. The energies of the HOMOs are equal (−4.76 eV) in **19**-C$_{60}$ and **20**. Furthermore, the results show that, at large donor-to-acceptor distances, the bridge retains the electronic communication due to super-exchange interactions mediated by low-energy orbitals.

However, even though such ground-state orbital interpreta-tions are appealing, simple arguments based on the Kohn–Sham orbitals may not be reflected exactly in the nature of the excited states. DFT does not reproduce charge separation in molecules well, so that we might also expect the above Kohn–Sham orbitals to be more deleocalized than would be found with other techniques. However, semiempirical configuration interaction (CI) calculations have proven to be very effective for such calculations. Therefore, singles-only CI (CIS) calculations with an active window of 20 occupied and 20 virtual orbitals and the AM1 Hamiltonian[21] as implemented in the VAMP 10.0[22] package were used to obtain a full description of the electronic states of the investigated systems. In the current context, we only address the charge-transfer states in **1**, **2**, **3**, pCp-C$_{60}$, **19**-C$_{60}$, and **20**. Note that, although these calculations were performed "in vacuo", the nature of the excited states (i.e., their degree of localization) does not usually change when solvent effects are simulated by a continuum solvent model, in contrast to some very polarizable ground-state radical ions. Only the relative energies of the states are affected. Beginning with the two C$_{60}$ references, pCp-C$_{60}$ and **19**-C$_{60}$, charge transfer states with dipole moment changes that depend on the distance between the positive and the negative charges were obtained. In all of these (see Figure S4, Supporting Information) the positive charge is localized on the bridge part adjacent to C$_{60}$. These intramolecular charge-transfer states correspond well with the orbital representations (Figure 2) and corroborate the hole-accepting features of the pCp-oPPVs, which make them reasonable electron donors. Furthermore, as predicted by the orbital discussion above, the charge transfer states in pCp-C$_{60}$ occur at higher energies due to the higher HOMO−LUMO gap, although the dipole moment changes are lower due to better electronic coupling between HOMO and LUMO. Importantly, this once more confirms the improvement of the electron donating properties of the Cp moieties in longer bridges. Populating the LUMO in **20**, which is relatively high in energy (−1.99 eV) as compared with C$_{60}$ (−3.04 eV in **19**-C$_{60}$) and localized on the ZnP, is energetically less favorable than in **19**-C$_{60}$. Hence, a less pronounced shift of electron density onto vacant orbitals of ZnP is observed and the corresponding change of dipole moment is reduced by a factor of nearly three. Summarizing, in addition to confirming the roles of ZnP and C$_{60}$ as the electron donor and acceptor, respectively, these results show the significant ability of the pCp-oPPVs to accept holes and donate electrons in the presence of energetically well-matched donors and acceptors.

Considering the ZnP-pCp-oPPV-C$_{60}$s (**1**, **2**, and **3**) the charge-transfer states obtained correspond well with the molecular orbitals shown in Figure 1. As seen from these orbital representations, charge transfer will occur from ZnP to C$_{60}$ in **1**, whereas in **2** and **3** an increasing contribution from the bridge states is evident. Consequently, for **1** the first four charge-transfer states obtained show the positive charge localized on the ZnP moiety with high changes of dipole moment in the range of 100 D. However, energetically separated by 0.3 eV from the other states a bridge charge transfer state with a $\Delta\mu$ value of 28 D was also obtained (Figure S3, Supporting Information). In **2**, on the other hand, only the first two states are pure HOMO to LUMO charge-transfer excitations with $\Delta\mu$ of 166 D due to the increased distance between the positive and negative charges. Following, two bridge charge-transfer excitations ($\Delta\mu$ = 61 D) mix with the

HOMO to LUMO transitions as a consequence of the mixing of the orbitals of ZnP and pCp-oPPV. The energy separation between the ZnP/C_{60} and pCp-oPPV/C_{60} charge-transfer states drops to 0.01 and 0.02 eV. Finally, in **3** the lowest energy charge-transfer transition stems from an intramolecular electron transfer between the bridge and C_{60} and exhibits a $\Delta\mu$ value of 60 D. Within the first five charge-transfer excitations, three correspond to pCp-oPPV to C_{60} charge-transfer processes and two to ZnP to C_{60} excitations with high changes of dipole moment ($\Delta\mu$ = 226 D). Importantly, all of these charge-transfer states are found in **3** within an energy range of only 0.13 eV.

Remarkably, the electrostatic potential mappings of the bridge states reveal that the positive charge invariably resides on the pCp-oPPV adjacent to C_{60}—Figure 3. This is due to the
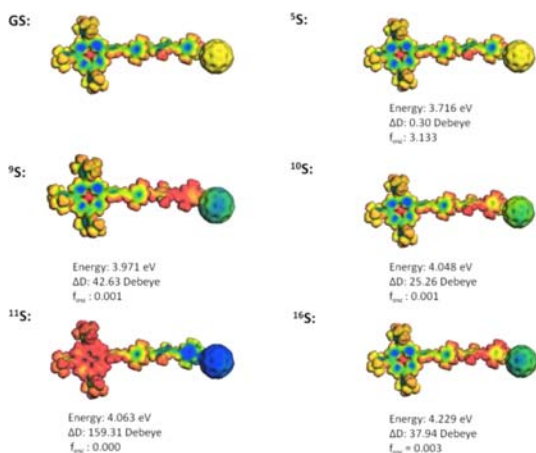

Figure 3. Molecular electrostatic potential projected onto the 0.017 e$^-$ Å^{-3} isodensity surfaces of the ground and selected excited states of **2**, mapped from −0.3 (blue) to 0.1 (red) Ha e^{-1}.

weaker donor character of the pCp-oPPVs as compared with ZnP. Hence, the charge separation remains stabilized only within a short distance between the donor and acceptor and represents an intermediate product within the ZnP to C_{60} electron-transfer process. Obviously, the stabilization of such intermediate charge-transfer states increases with increasing bridge length. This, in turn, may increase their lifetimes and make it feasible to detect them by time-resolved spectroscopic methods.

Most importantly, the pCp-oPPVs act mainly as hole transporters because of their energetically high-lying occupied orbitals. The role of the bridge is restricted to mediating the electronic coupling between the ZnP and C_{60} (vide infra). However, as seen from the CI calculations, increasing the length of the bridge stabilizes these intermediate states more and more and makes them energetically accessible. Hence, in **2** and **3**, the bridge excitations mix with the main HOMO to LUMO charge transfer. Therefore, a change of charge-transfer mechanism may be expected upon increasing temperature or length of the linker. In **1**, where charge delocalization is less pronounced than in **2** and **3**, a coherent tunneling process presumably governs the charge transfer, whereas going from **2** to **3** the probability of observing a subsequent charge hopping from the ZnP to the bridge and from the bridge to C_{60} increases.

Figure 3 shows the molecular electrostatic potential of the ground and selected singlet excited states of **2**, mapped onto

electron density isosurfaces. These states are representative for the different photophysical processes that may occur. The local excitation of ZnP (^5S) features high oscillator strength and practically no shift in charge density. At higher energies, several states display a charge shift from pCp to C_{60}, with relatively low oscillator strengths (^9S, ^{10}S, and ^{16}S). The direct excitation into a $ZnP^{\bullet+}$-pCp-oPPV-$C_{60}^{\bullet-}$ radical ion pair state (^{11}S) is impossible owing to the weak orbital overlap, which leads to zero oscillator strength. Therefore, this state may only be populated from another excited state.

In summary, the calculations clearly suggest that the charge transfer is effectively mediated by the pCp-oPPVs with a predominant hole-transfer mechanism. Delocalization and trapping of the holes may occur only upon strong electronic interactions between the electron donating and electron accepting orbitals. These interactions are mainly governed by the distance between electron donor and electron acceptor. However, these are effectively present due to the efficient electronic communication, even over a distance of more than 48 Å, as found for **3**.

Absorption and Fluorescence Spectroscopy. In the absorption spectra, the Soret and Q-Bands of ZnP at 430 nm and 550/604 nm, respectively, of **1**, **2**, and **3** dominate the visible part—Figure 4. The characteristic absorptions of C_{60}
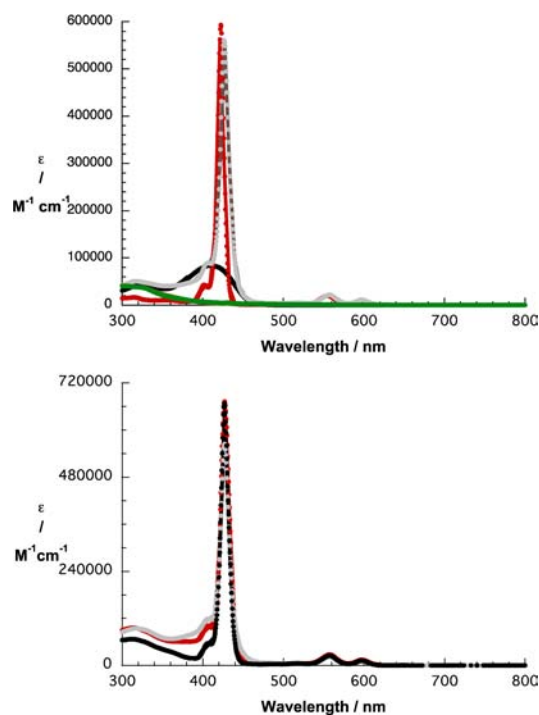

Figure 4. Upper part—room temperature absorption spectra of **19** (black), **20** (gray), ZnP (red), N-methyl-pyrrolidino[3,4:1,2][60]-fullerene (NMPC$_{60}$) (dark yellow), and pCp-C$_{60}$ (green) in THF. Lower part—room temperature absorption spectra of **1** (black), **2** (gray), and **3** (red) in THF.

and pCp-oPPV, on the other hand, evolve in the ultraviolet part. In particular, C_{60} absorbs between 250 and 300 nm, whereas the pCp-oPPVs exhibit broad maxima between 300 and 450 nm. A closer look at the position of the Soret and Q bands reveals a red shift of about 20 nm for **1**, **2**, and **3** relative to ZnP.

Further insights into the origin of these absorptions came from complementary investigations with references **12**, **18**, and **19**—Figure S5 (Supporting Information). Important is the fact that the overall absorption characteristics depend on the number and the positioning of the pCps. In particular, the absorption spectra of all references reveal two main features, that is, a rather broad band between 300 and 360 nm and a rather sharp band in the 370−450 nm region. The 300−360 nm bands correlate with oPPV centered transitions, whereas the 370−450 nm bands relate to transitions that are centered on pCp. Interestingly, when comparing **18** with **19** blue-shifted oPPV absorptions evolve in the presence of more than a single pCp. In particular, blue-shifts evolve from 340 to 325 nm for **18** versus **19**. The blue shift seen in the oPPV transitions infers that an increasing number of pCps interrupts the oPPV π-conjugation. In other words, the through-bond oPPV conjugation is broken and replaced by the through-space pCp conjugation. Despite the aforementioned, the red-shift from 406 to 411 nm of the pCp absorption in **12** and **19** as the overall length increases corroborates that the π-conjugation is intact but depends on the oPPV conjugation length. As such, it is safe to assume that the electronic coupling between oPPVs and pCps is rather strong.

With this information in hand, we are able to dissect the absorption features in the electron donor−acceptor conjugates **1**, **2**, and **3**. oPPV absorptions are discernible between 300 and 350 nm, whereas the pCp absorptions are masked by the much stronger absorbing Soret band of ZnP. In fact, they appear as features that are superimposed on the Soret band. Variation of the solvent from toluene to THF and benzonitrile hardly affects the positions of the oPPV and pCp maxima. Equally important is that altering the length of the molecular wires affords appreciable changes. Taken the aforementioned into concert, the spectral results suggest the lack of extended conjugation throughout the corresponding molecular wires. Thus, inserting several through-space conjugated pCps into **12** and **19**, and into **2** and **3** lowers, on one hand, the oPPV π-conjugation but maintains, on the other hand, the electronic communication through the molecular wires.

In order to explore the aspect of through-space versus through-bond conjugation, steady-state and time-resolved emission as well as transient absorption measurements were performed.

All three of the redox-active constituents, that is, ZnP, pCp-oPPV, and C_{60}, emit singlet excited state energy in different spectral regions of the spectrum. For example, 420 nm excitation leads to a rather strong ZnP fluorescence ($\Phi = 4.0 \times 10^{-2}$) between 570 and 700 nm—Figure 5—whereas the pCp-oPPV fluorescence ($\Phi = 1.1 \times 10^{-1}$) maximizes around 466 nm—Figure S6 (Supporting Information)—upon 350 nm excitation. The characteristic but weak C_{60} singlet excited state fluorescence ($\Phi = 6.0 \times 10^{-4}$) evolves around 710 nm upon 350 nm excitation. In **1**, **2**, and **3**, the ZnP emission is quenched upon ZnP excitation at, for example, 420 nm. The quantum yields—in THF: 4.3×10^{-3} for **1**, 2.7×10^{-2} for **2**, and 3.1×10^{-2} for **3**—imply a rather weak but evident quenching. Additionally, a comparison of the quantum yields in solvents of different polarities (Table 1) reveals an even weaker dependence on solvent polarity—vide infra.

Hence, it seems that the excited state interactions between the strongly fluorescent and electron donating ZnP and the electron accepting C_{60} are rather weak. As a matter of fact, an energy transfer from the photoexcited ZnP to C_{60} as the sole
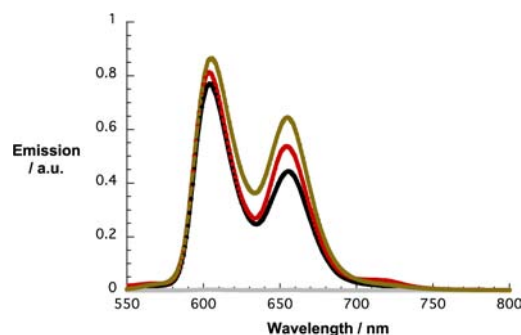

Figure 5. Room temperature fluorescence spectra of ZnP (dark yellow), **1** (gray), **2** (black), and **3** (red) in THF solutions that reveal the same absorption of 0.2 at the 420 nm excitation.

deactivation pathway is ruled out on the basis of complementary TCSPC fluorescence lifetime measurements. The corresponding fluorescence lifetimes upon 403 nm excitation with values for **2** of 1.68×10^{-9} s in toluene, 1.44×10^{-9} s in THF, and 1.44×10^{-9} s in benzonitrile as well as for **3** of 1.90×10^{-9} s in toluene, 1.79×10^{-9} s in THF, and 1.70×10^{-9} s in benzonitrile reflect the steady-state fluorescence experiments. In particular, the dependence on solvent polarity and on the length of the pCp-oPPVs is reconfirmed. In line with recent experiments,[13] this indicates a charge transfer as deactivation pathway. Finally, comparing the pCp-oPPV fluorescence upon 350 nm excitation in **19** and **20** reveals a significant fluorescence quenching, and a sensitized porphyrin fluorescence—Figure S6 (Supporting Information)—upon 350 nm excitation.

Transient Absorption Spectroscopy. Thus, to work out the contributions from energy and/or charge transfer to the overall deactivation processes, we employed complementary transient absorption measurements. To this end, excitation at 387 nm of argon-saturated THF solutions of the references **12** and **19** leads to an instantaneous formation of their singlet−singlet absorptions characterized by transient bleaching at 400 and 530 nm and broad transient maxima at 640 and 860 nm—Figure 6.

Representative differential absorption spectra for ZnP, taken after laser excitation at 387 or 420 nm in toluene solution, are displayed in Figure S7 of the Supporting Information. The differential spectrum recorded immediately after the laser pulse is characterized by bleaching of the porphyrin Q-band absorption at 560 nm and appearance of transients at 480 nm and between 580 and 750 nm. These are spectral attributes of the ZnP singlet excited state (2.04 eV), which decays slowly (4.0×10^{8} s^{-1}) in toluene to the energetically lower-lying ZnP triplet excited state (1.53 eV) via intersystem crossing. Now, considering the transient spectra of **20**—Figure 6—the observation of an instantaneous growth of a broad absorption between 570 and 750 nm affirms selective excitation of the ZnP. In addition, the singlet excited state features of pCp-oPPV are discernible. The relative ratio depends on the excitation wavelength with 387 nm that favors pCp-oPPV excitation and 420 nm that leads predominantly to ZnP excitation. In **20**, the pCp-oPPV centered singlet−singlet absorptions decay, however, with accelerated dynamics of less than 2 ps. The latter transform rapidly to the corresponding ZnP singlet excited state. Owing to the fact that the ZnP singlet excited state is not appreciably impacted by the presence of pCp-oPPV, the pCp-oPPV to ZnP energy transfer is followed by intersystem

Table 1. Quantum Yields (Φ_f), Charge Separation (k_{CS}) Rate Constants, Charge Recombination (k_{CR}) Rate Constants, and Fluorescence Lifetimes (τ_{TCSPC} and τ_{SS}) of 1, 2, 3, and Their References in Various Solvents

	solvent	Φ_f	k_{CS} (s^{-1})	k_{CR} (s^{-1})	$\tau_{SS}{}^a$ (ns)	$\tau_{TCSPC}{}^b$ (ns)
ZnP[c]		0.04			2.4	2.4
1[c]	toluene					
	THF	0.004	5.2×10^9	1.0×10^6	0.20	0.22
	PhCN					
2[c]	toluene	0.028	6.2×10^8		1.65	1.68
	THF	0.027		2.6×10^7	1.65	1.44
	PhCN	0.025			1.51	1.48
3[c]	toluene	0.030	5.2×10^8		1.81	1.90
	THF	0.031		2.7×10^7	1.84	1.79
	PhCN	0.024			1.44	1.70
12[d]	THF	0.71				
15[d]	THF	0.20				
18[d]	THF	0.57				
19[d]	THF	0.70				
20[d]	THF	0.024				
N-methyl-pyrrolidino[3,4:1,2][60]fullerene (NMPC$_{60}$)[e]		6×10^{-4}			1.2	1.2

[a]Lifetimes calculated from steady-state emission via equation $k_{CS} = [(\Phi(\text{reference}) - (\Phi(\text{conjugate}))/[\tau(\text{reference}) \cdot \Phi(\text{conjugate})]$ (1). [b]Lifetimes determined by TCSPC experiments. [c]Excited at 420 nm. [d]Excited at 350 nm. [e]Excited at 350 nm.
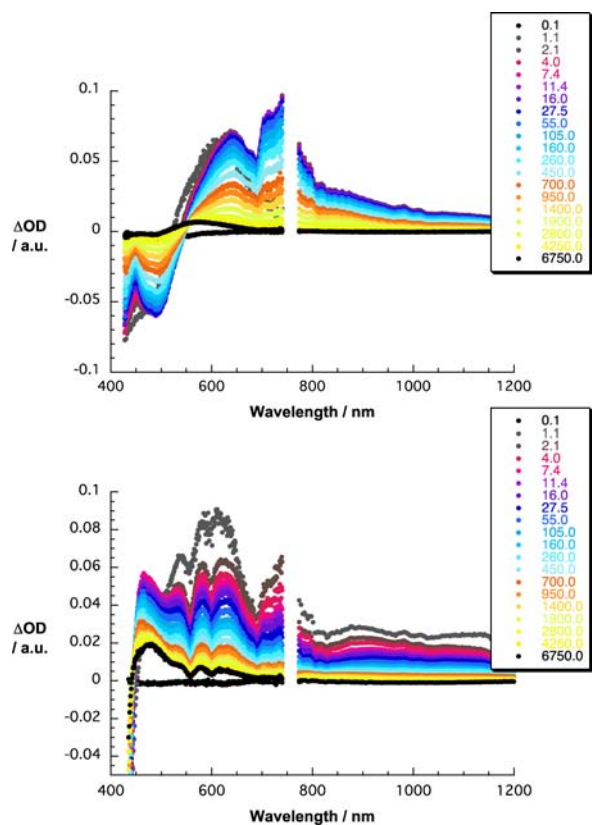

Figure 6. Upper part—differential absorption spectra (visible and near-infrared) obtained upon femtosecond flash photolysis (387 nm, 110 nJ) of **19** in argon saturated THF with several time delays between 0 and 6750 ps at room temperature. Lower part—differential absorption spectra (visible and near-infrared) obtained upon femtosecond flash photolysis (387 nm, 110 nJ) of **20** in argon saturated THF with several time delays between 0 and 6750 ps at room temperature.

crossing to the corresponding ZnP triplet excited state, namely broad transients that maximize around 840 nm. Notably, the

overall broadening of the bands results from an overlap between ZnP and pCp-oPPV absorptions.

In pCp-C$_{60}$, at early times, the differential absorption spectra upon 387 nm excitation are practically identical to those seen with C$_{60}$, that is, a broad transient at 900 nm, attesting to the formation of the C$_{60}$ singlet excited state—Figure 7. In the C$_{60}$
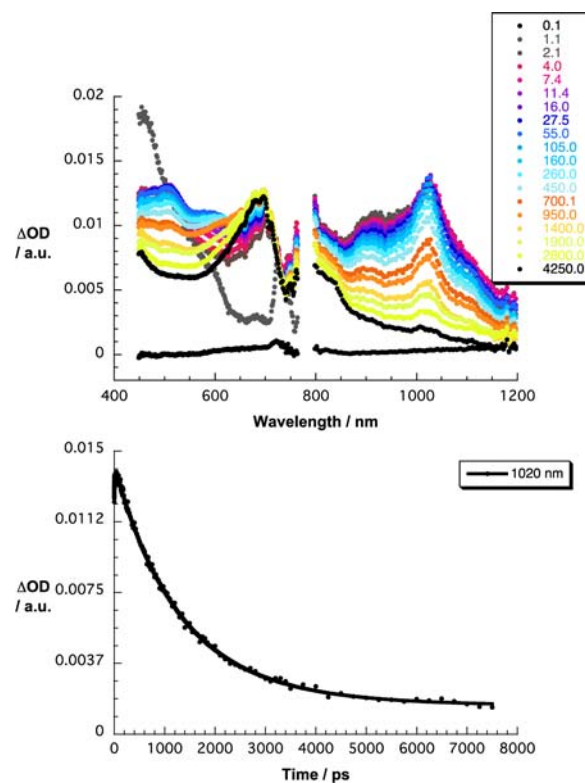

Figure 7. Upper part—differential absorption spectra (visible and near-infrared) obtained upon femtosecond flash photolysis (387 nm, 200 nJ) of pCp-C$_{60}$ in argon saturated THF with several time delays between 0.1 and 4250 ps at room temperature. Lower part—time absorption profile at 1020 nm monitoring the charge separation and charge recombination dynamics.

reference, intersystem crossing (5.0×10^8 s^{-1}) to the energetically lower lying C_{60} triplet dominates the deactivation of the singlet excited state of C_{60}. In stark contrast to C_{60}, after a delay time of ca. 25 ps, a new transition around 510 nm starts to grow in for pCp-C_{60}. This is accompanied by appearance of an absorption in the near-infrared region around 1000 nm, whose formation is completed within 30 ps. Based on spectral comparisons, the former is ascribed to the pCp π-radical cation (pCp$^{\bullet+}$), while the latter is due to the C_{60} π-radical anion ($C_{60}^{\bullet-}$). Charge recombination dynamics were analyzed by following the absorption decay of the reduced form of C_{60} and of the oxidized form of pCp, yielding a lifetime of 1300 ps in THF.

Finally, turning to the ZnP-pCp-oPPV-C_{60}s (**1**, **2**, and **3**), a differentiation between 420 and 387 nm excitation should be made. Considering the light partition in **1**, **2**, and **3** at 420 and 387 nm, ZnP absorbs exclusively at the earlier wavelength, while at the latter the ZnP to C_{60} absorption ratio is 1:1. Upon 420 nm excitation of **1**, **2**, and **3**, the instantaneous formation of transient spectra is discernible that resemble those of the ZnP singlet excited state despite the presence of C_{60}—Figures 7 and 8. Here, the ZnP singlet excited state features decay on the time
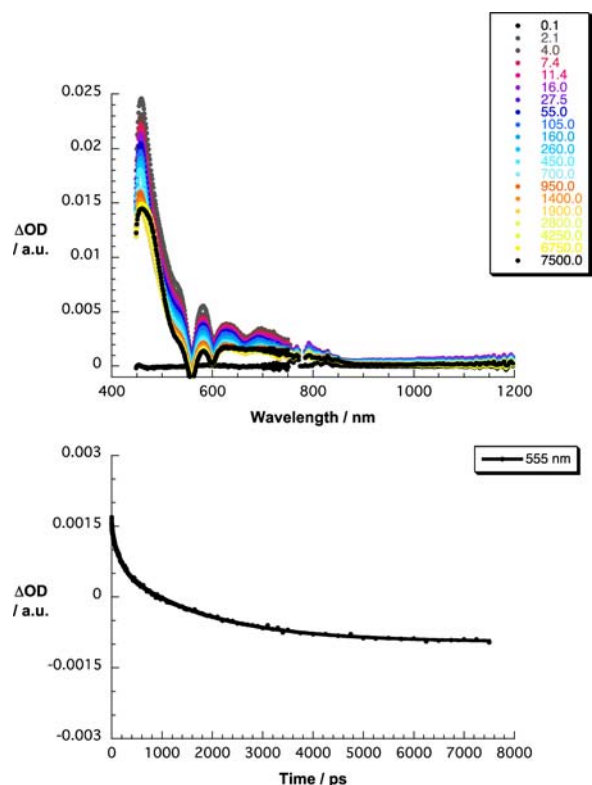

Figure 8. Upper part—differential absorption spectra (visible and near-infrared) obtained upon femtosecond flash photolysis (420 nm, 100 nJ) of **2** in argon saturated toluene with several time delays between 0.1 and 7500 ps at room temperature. Lower part—time absorption profiles at 555 nm monitoring the charge separation dynamics.

scale of up to 8 ns with lifetimes that range, for example, in THF from 0.2 for **1** and 1.65 for **2** to 1.84 ns for **3**. These values are comparable to those determined in the time-resolved fluorescence measurements. Interesting is that at the end of the 8 ns time scale the ZnP triplet excited state features dominate the differential absorption spectrum. From the latter we infer

that the competition between ZnP intersystem crossing and ZnP$^{\bullet+}$-pCp-oPPV-$C_{60}^{\bullet-}$ charge transfer must be heavily on the earlier side. Still, spectroscopic evidence for ZnP$^{\bullet+}$-pCp-oPPV-$C_{60}^{\bullet-}$—vide infra—suggests that electron tunneling is operative in **2** and **3**.

In sharp contrast, exciting **1**, **2**, and **3** at 387 nm leads besides ZnP centered singlet excited state characteristics (vide supra) to C_{60} centered singlet excited-state features. In terms of C_{60}, the presence of ZnP and pCp-oPPV suppresses the C_{60} centered intersystem crossing and seems to favor a decay with, for example, 6.2×10^8 s^{-1} for **2** and 5.2×10^8 s^{-1} for **3** in THF. It is the radical ion pair state that is formed. Evidence for the radical ion pair state formation comes from maxima in the visible (i.e., 510 nm) and in the near-infrared regions (i.e., 1000 nm). The features in the visible correspond, however, to the pCp π-radical cation (pCp$^{\bullet+}$) rather than to the ZnP π-radical cation (ZnP$^{\bullet+}$), whereas in the near-infrared region the 1000 nm maximum agrees well with those of the C_{60} π-radical anion ($C_{60}^{\bullet-}$). Important criteria are the kinetic resemblance between the decay of the C_{60} singlet excited state and the growth of ZnP-(pCp-oPPV)$^{\bullet+}$-$C_{60}^{\bullet-}$ radical ion pair state. Evidently, the deactivation of the singlet excited state in **2** and **3** leads exclusively to a charge transfer between pCp and C_{60} without giving rise to a subsequent charge shift to yield the ZnP$^{\bullet+}$-pCp-oPPV-$C_{60}^{\bullet-}$ radical ion pair state. Such a charge shift would be endergonic due to the unfavorable ZnP oxidation. In terms of ZnP, the same slow deactivation of the ZnP singlet excited state that developed during the 420 nm excitation experiments— vide supra—affords the ZnP$^{\bullet+}$-pCp-oPPV-$C_{60}^{\bullet-}$ radical ion pair state.

To gather evidence for the ZnP$^{\bullet+}$-pCp-oPPV-$C_{60}^{\bullet-}$ radical ion pair state formation and its decay we turned to nanosecond flash photolysis experiments—Figure 9. Thereby, 532 nm excitation rather than 355 nm excitation was used to ensure mainly ZnP excitation of **2** and **3**. Immediately after the laser excitation a weak but appreciable absorption, especially in the near-infrared region, is registered. In argon-saturated THF the decay is biexponential. On the early time scale it is monomolecular, while on the longer time scale it is bimolecular. Turning to experiments that were performed in oxygen saturated THF, the earlier decay is marginally affected, while the latter decay is heavily quenched. From this we conclude that the long-lived species must be the ZnP triplet excited state. Spectroscopic support for this postulate comes from the 840 nm marker. In sharp contrast, the C_{60} π-radical anion is the dominating species with its 1000 nm marker during the early times. Notably, the competition between ZnP intersystem crossing/ZnP triplet excited state growth and ZnP$^{\bullet+}$-pCp-oPPV-$C_{60}^{\bullet-}$ radical ion pair state formation is heavily on the earlier side. Still, a small fraction of the latter is formed. In other words, a moderately efficient, but long-lived, ZnP$^{\bullet+}$-pCp-oPPV-$C_{60}^{\bullet-}$ radical ion pair state is formed. This is in sound agreement with the slightly quenched ZnP centered fluorescence in **2** and **3**. In terms of ZnP$^{\bullet+}$-pCp-oPPV-$C_{60}^{\bullet-}$ radical ion pair state lifetime, values of ~260 ± 40 ns were reached for **2** and **3**.

Mechanistic Aspects. Relating the charge separation dynamics upon 420 nm ZnP excitation in THF to the electron donor–acceptor separation (i.e., center-to-center distance, R_{CC}) enables us to evaluate the damping factor of the pCp-oPPV bridges. The overall relationship reveals a nonlinear dependence for the charge separation for the three ZnP-pCp-oPPV-C_{60}s (**1**, **2**, and **3**). In particular, rather strong distance
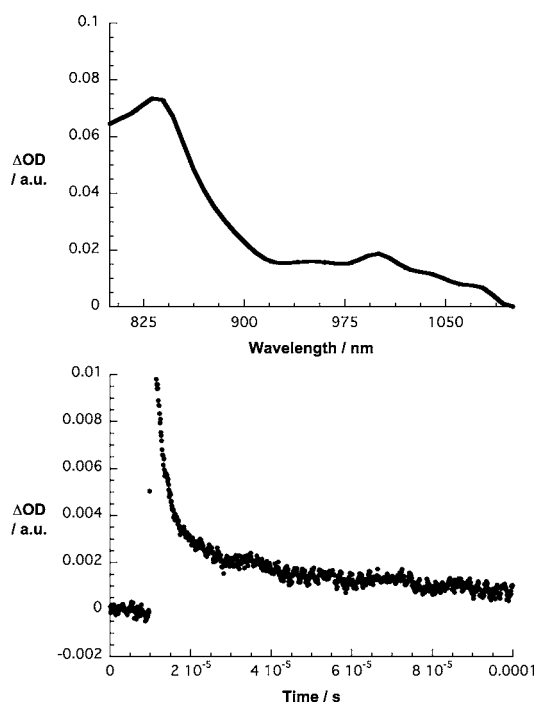
Figure 9. Upper part—differential absorption spectra (visible and near-infrared) obtained upon nanosecond flash photolysis (532 nm, 10 mJ) of **2** in argon saturated THF with a time delay of 275 ns at room temperature. Lower part—time absorption profile at 1000 nm monitoring the charge recombination dynamics. Please note that the oscillations may be artifact due to the lamp pulser.

dependence for **1** and **2** is followed by weak distance dependence for **2** and **3**. The former give a damping factor of 0.145 Å^{-1} and the latter a value of 0.012 Å^{-1}. Notably, 0.012 Å^{-1} is in perfect agreement with what we have established earlier for oPPV bridges (i.e., 0.01 ± 0.005 Å^{-1}).[10c] 0.145 Å^{-1}, on the other hand, is nearly a magnitude larger.

To shed light onto the charge transfer mechanisms in **1**, **2**, and **3** yielding ZnP$^{\bullet+}$-pCp-oPPV-C$_{60}$$^{\bullet-}$, we probed the temperature dependence of the ZnP fluorescence quenching in *ortho*-dichlorobenzene and benzonitrile in the range from 273 to 338 K—Figure 10. Here, we used the fluorescence quantum yields to extrapolate the rate constants for charge separation at each temperature and treated them in the Arrhenius formalism, that is, plotting $\ln(k_{CS})$ versus T^{-1}.
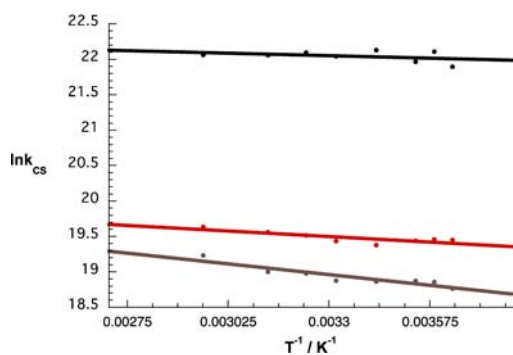

Figure 10. Temperature dependence of the charge separation rate constants for **1** (black), **2** (red), and **3** (grey) in the 273−338 K regime based on the temperature-dependent fluorescence experiments in benzonitrile.

Overall, the rate constants do not vary in *ortho*-dichlorobenzene and benzonitrile. Obviously, a superexchange mechanism is the modus operandi. In the high temperature range (i.e., > 30 °C) the rate constants increase. Therefore, we can conclude that a superexchange mechanism dominates the charge separation in all our experiments as they were carried out at room temperature. Independent confirmation for the aforementioned came from an analysis of ZnP singlet excited features in benzonitrile in the range from 280 to 334 K (Figure 11). Overall, activation barriers of 1.0, 4.4, and 6.1 kJ/mol for **1**, **2**, and **3**, respectively, corroborate the superexchange mechanism.
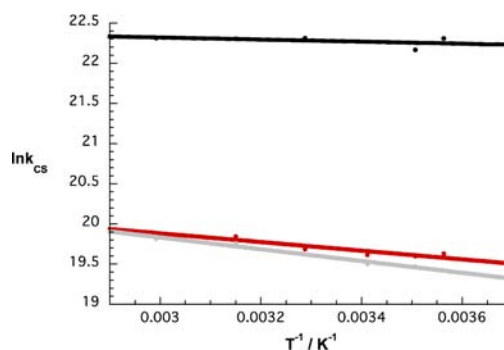

Figure 11. Temperature dependence of the charge separation rate constants for **1** (black), **2** (red), and **3** (grey) in the 280 and 334 K regime based on the temperature-dependent femtosecond transient absorption experiments in benzonitrile.

CONCLUSIONS

We have carried out the synthesis of a series of ZnP-pCp-oPPV-C$_{60}$ conjugates covalently connected through [2,2′]-paracyclophane-oligophenylenevinylene (pCp-oPPV) bridges containing one, two, and three pCps.

Molecular modeling studies have shown that due to the strong electron-accepting properties of C$_{60}$, a charge transfer occurs between C$_{60}$ and the adjacent pCp. As already shown in a preliminary work,[13] these states may act as intermediate steps in the charge transfer process. Their stability originates from the fact that the changes of the dipole moment are small, which is simultaneously the reason why only the pCp unit closest to C$_{60}$ is oxidized in **2** and **3**. Importantly, the occurrence and stability of these intermediate low-energy charge transfer states ratifies their extremely long lifetimes. They mix electronically with the ZnP$^{\bullet+}$-pCp-oPPV-C$_{60}$$^{\bullet-}$ radical ion pair states, which leads to an overall increase in stability of the charge separated state. This nicely complies with the results from recent work with pCp-oPPV bridges, where we have shown that, when assuming that hole transport dominates charge transport in π-conjugated molecular wires, a lack of delocalization across the pCp linkers will certainly preclude strong electronic communication between the electron donor and acceptor.

ZnP excitation of **1**, **2**, and **3** results in a rather slow charge transfer between ZnP and C$_{60}$, at which end the ZnP$^{\bullet+}$-pCp-oPPV-C$_{60}$$^{\bullet-}$ radical ion pair state evolves. Notably, C$_{60}$ excitation of **1**, **2**, and **3** leads exclusively to a charge transfer between pCp and C$_{60}$ without giving rise to a subsequent charge shift to yield the ZnP$^{\bullet+}$-pCp-oPPV-C$_{60}$$^{\bullet-}$ radical ion pair state. Temperature-dependent ZnP singlet excited state decays, that is, fluorescence and transient absorption experiments, corroborate that in the low temperature range (i.e., < 30 °C) the rate constants are invariable. Here, a superexchange

mechanism is the modus operandi. Moreover, relating the charge separation dynamics to the electron donor−acceptor separation enabled us to evaluate the damping factor of the pCp-oPPV bridges. To this end, a rather strong distance dependence for **1** and **2** featuring a damping factor of 0.145 Å is followed by weak distance dependence for **2** and **3** with a value of 0.012 Å^{-1}.

■ ASSOCIATED CONTENT

Ⓢ Supporting Information

Experimental procedures with complete spectroscopic and structural analysis, including supporting figures and tables. This material is available free of charge via the Internet at http://pubs.acs.org.

■ AUTHOR INFORMATION

Corresponding Author
guldi@chemie.uni-erlangen.de; nazmar@quim.ucm.es

Author Contributions
[⊥]These authors contributed equally to this work

Notes
The authors declare no competing financial interest.

■ ACKNOWLEDGMENTS

■ REFERENCES

(1) (a) Cannon, R. D. *Electron Transfer Reactions*; Butterworths: London, U.K., 1980. (b) Eberson, L. *Electron Transfer Reactions in Organic Chemistry*; Springer: New York, 1987.

(2) Gust, D.; Moore, T. A.; Moore, A. L. *Acc. Chem. Res.* **2001**, *34*, 40−48.

(3) Imahori, H. *Bull. Chem. Soc. Jpn.* **2007**, *80*, 621.

(4) Kira, A.; Umeyama, T.; Matano, Y.; Yoshida, K.; Isoda, S.; Park, J. K.; Kim, D.; Imahori, H. *J. Am. Chem. Soc.* **2009**, *131*, 3198.

(5) Liddell, P. A.; Kuciauskas, D.; Sumida, J. P.; Nash, B.; Nguyen, D.; Moore, A. L.; Moore, T. A.; Gust, D. *J. Am. Chem. Soc.* **1997**, *119*, 1400.

(6) Kuciauskas, D.; Liddell, P. A.; Lin, S.; Johnson, T. E.; Weghorn, S. J.; Lindsey, J. S.; Moore, A. L.; Moore, T. A.; Gust, D. *J. Am. Chem. Soc.* **1999**, *121*, 8604.

(7) (a) Guldi, D. M. *Chem. Soc. Rev.* **2002**, *31*, 22. (b) Drain, C. M.; Varotto, A.; Radivojevic, I. *Chem. Rev.* **2009**, *109*, 1630. (c) Holten, D.; Bocian, D. F.; Lindsey, J. S. *Acc. Chem. Res.* **2002**, *35*, 57.

(8) (a) Imahori, H.; Sakata, Y. *Adv. Mater.* **1997**, *9*, 537. (b) Echegoyen, L.; Echegoyen, L. E. *Acc. Chem. Res.* **1998**, *31*, 593. (c) Guldi, D. M. *Chem. Commun.* **2000**, *5*, 321. (d) Prato, M.; Guldi, D. M. *Acc. Chem. Res.* **2000**, *33*, 695−703. (e) Echegoyen, L.; Diederich, F.; Echegoyen, L. E. In *Fullerenes: Chemistry, Physics, and Technology*; Kadish, K. M., Ruoff, R. S., Eds.; Wiley-IEEE: New York, 2000; p20.

(9) (a) Ikemoto, J.; Takimiya, K.; Aso, Y.; Otsubo, T.; Fujitsuka, M.; Ito, O. *Org. Lett.* **2002**, *4*, 309. (b) Vail, S. A.; Krawczuk, P. J.; Guldi, D. M.; Palkar, A.; Echegoyen, L.; Tome, J. P. C.; Fazio, M. A.; Schuster, D. I. *Chem.—Eur. J.* **2005**, *11*, 3375. (c) MacMahon, S.; Fong, R., II;

Baran, P. S.; Safonov, I.; Wilson, S. R.; Schuster, D. I. *J. Org. Chem.* **2001**, *66*, 5449.

(10) (a) Giacalone, F.; Segura, J. L.; Martín, N.; Guldi, D. M. *J. Am. Chem. Soc.* **2004**, *126*, 5340. (b) de la Torre, G.; Giacalone, F.; Segura, J. L.; Martín, N.; Guldi, D. M. *Chem.—Eur. J.* **2005**, *11*, 1267. (c) Atienza, C.; Martin, N.; Wielopolski, M.; Haworth, N.; Clark, T.; Guldi, D. M. *Chem. Commun.* **2006**, *43*, 3202. (d) Atienza-Castellanos, C.; Wielopolski, M.; Guldi, D. M.; van der Pol, C.; Bryce, M. R.; Filippone, S.; Martin, N. *Chem. Commun.* **2007**, *43*, 5164. (e) Molina-Ontoria, A.; Fernández, G.; Wielopolski, M.; Atienza, C.; Sánchez, L.; Gouloumis, A.; Clark, T.; Martín, N.; Guldi, D. M. *J. Am. Chem. Soc.* **2009**, *131*, 12218.

(11) (a) Nitzan, A.; Ratner, M. A. *Science* **2003**, *300*, 1384. (b) Geise, B.; Amaudrut, J.; Kohler, A. K.; Spormann, M.; Wassely, S. *Nature* **2001**, *412*, 318. (c) Davis, W. B.; Svec, W. A.; Ratner, M. A.; Wasielewski, M. R. *Nature* **1998**, *396*, 60. (d) Choi, S. H.; Kim, B.-S.; Frisbie, D. C. *Science* **2008**, *320*, 1482.

(12) (a) Marcus, R. A. *J. Chem. Phys.* **1956**, *24*, 966. (b) Marcus, R. A. *J. Chem. Phys.* **1956**, *24*, 979. (c) Marcus, R. A. *J. Chem. Phys.* **1957**, *26*, 867. (d) Marcus, R. A. *J. Chem. Phys.* **1957**, *26*, 872. (e) Marcus, R. A. *Can. J. Chem.* **1959**, *37*, 155.

(13) Molina-Ontoria, A.; Wielopolski, M.; Gebhardt, J.; Gouloumis, A.; Clark, T.; Guldi, D. M.; Martin, N. *J. Am. Chem. Soc.* **2011**, *133*, 2370.

(14) (a) James, D. K.; Tour, J. M. *Top. Curr. Chem.* **2005**, *257*, 33. (b) Weiss, E. A.; Wasielewski, M. R.; Ratner, M. A. *Top. Curr. Chem.* **2005**, *257*, 103. (c) Guldi, D. M.; Illescas, B. M.; Atienza, C. M.; Wielopolski, M.; Martín, N. *Chem. Soc. Rev.* **2009**, *38*, 1587.

(15) (a) Prato, M.; Maggini, M. *Acc. Chem. Res.* **1998**, *31*, 519−526. (b) Tagmatarchis, N.; Prato, M. *Synlett.* **2003**, *15* (6), 768.

(16) Wolfrum, S.; Pinzón, J. R.; Molina-Ontoria, A.; Gouloumis, A.; Martín, N.; Echegoyen, L.; Guldi, D. M. *Chem. Commun.* **2011**, *47*, 2270.

(17) Stephens, P. J; Devlin, F. J; Chablowski, C. F; Frisch, M, J. *Phys. Chem.* **1994**, *98*, 11623.

(18) Rassolov, V. A; Pople, J. A; Ratner, M. A; Windus, T. L *J. Chem. Phys.* **1998**, *109*, 1223.

(19) Frisch, M. J., et al. Gaussian, Inc.: Wallingford, CT, 2009.

(20) **19**-C$_{60}$ is a model molecule used only for theoretical calculations:

19-C$_{60}$
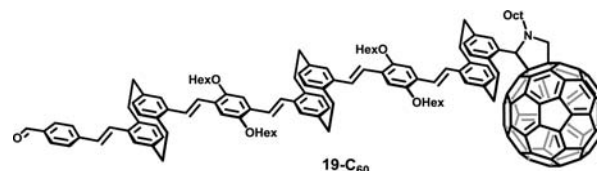
(21) Dewar, M. J. S.; Zoebisch, E. G.; Healy, E. F.; Stewart, J. J. P. *J. Am. Chem. Soc.* **1985**, *107*, 3902.

(22) Clark, T.; Alex, A.; Beck, B.; Burkhardt, F.; Chandrasekhar, J.; Gedeck, P.; Horn, A.; Hutter, M.; Martin, B.; Rauhut, G.; Sauer, W.; Schindler, T.; Steinke, T. *Computer-Chemie-Centrum*; Universität Erlangen-Nürnberg: Erlangen, 2003.